Measurement and Modeling of N-Atom Behavior in the Afterglow of a Microwave Plasma

Ta-Chin Wei, Lance R. Collins, and Jonathan Phillips
Dept. of Chemical Engineering, The Pennsylvania State University, University Park, PA 16802

Nitrogen-atom behavior in a low-pressure, nonisothermal microwave-generated nitrogen afterglow was studied. N-atom flux was measured by chemical titration. It was found that an increase in power or flow rate, or a decrease in pressure resulted in larger productions of N atoms. A one-dimensional mass-continuity equation was used to model N atoms' concentration field in the afterglow. The model, with no adjustable parameters, agreed closely with experimental measurements. The model shows that convection, diffusion, and wall recombination play important roles in the afterglow. In contrast, N-atom generation and homogeneous recombination are of marginal importance. The model was manipulated to assess the impact of the measuring technique, chemical titration, on the N-atom flux. It was found that the N-atom flux profile is only slightly impacted, although the concentration profile is strongly modified.

Introduction

Historically the greatest value derived from the study of afterglow plasmas has been the determination of rate constants for radical reactions: values that have added greatly to the fundamental understanding of reaction chemistry (Harteck et al., 1958; Herron et al., 1959; Kretschmer and Petersen, 1963). These values are also crucial to modern modeling studies, including models of atmospheric chemistry (Mellouki et al., 1987) and combustion chemistry (Hochgreb and Dryer, 1992; Markatou et al., 1993).

The focus of studies of afterglow plasmas has recently shifted from their use as scientific tools, to their use as industrial reactors. In fact, afterglow reactors are now found in virtually all integrated circuit "fabs" (Graves, 1989). One of the greatest advantages of reactors of this type is that they provide high radical concentrations with low ion concentrations, at a low temperature. Often, high radical concentrations are required for the desired chemistry (etching, oxidation, deposition), and high-energy ions are unwanted, as they tend to cause material damage (Nichollian and Brews, 1980; Dautremont-Smith, 1987). Low temperatures are generally desirable to reduce the rate of solid-state diffusion, which clearly can destroy the carefully constructed submicron zones found in integrated circuits.

The new applications of afterglow reactors require models more sophisticated than most currently available. Generally, available models apply only to low radical concentration, constant-temperature regions of the afterglow; moreover, interactions between charged-particle and neutral subsystems are neglected. New models must reflect the environment found in industrial settings: high radical concentrations, sharp temperature gradients, and charged-particle and neutral species subsystems that are not in equilibrium. It must also be understood that the two basic subsystems in an afterglow are distinct in terms of fluid mechanics, yet interact kinetically to significantly impact each other.

Recent, and more complete, models of the neutral-species and charged-species components of oxygen afterglows, with no adjustable parameters, accurately reflect experimentally measured charged-species and neutral-species flux and concentration profiles (Chou et al., 1992). The models also give quantitative insight into the relative importance of different mechanisms of mass transport, the effect of measuring techniques on the plasma, the relative importance of wall and homogeneous reaction mechanisms, and the impact of the interactions between the neutral-species and charged-particle subsystems.

In the present study a model of the afterglow region of a nitrogen plasma that includes both diffusion and convection as well as accounting for temperature gradients and high radical concentrations is developed. The model is then compared with experimental data collected over a range of operating pressures, flow rates, and levels of power adsorption.

Correspondence concerning this article should be addressed to J. Phillips.

Plasmas of this type are not as widely used industrially as oxygen afterglow, but there are a number of potentially valuable applications. Indeed, there is increased interest in creating nitrided thin films. Nitrides of III–V semiconductors are promising materials for electronics and optical devices (Strite and Morkoc, 1992; Sun and Ekerdt, 1993). Nitrogen afterglow can be used for steel surface nitriding (Ricard et al., 1990; Bougdira et al., 1991). Also nitrogen plasmas could be used to create carbon nitrides (Han and Feldman, 1988; Niu et al., 1993), very hard materials that have been shown to have excellent tribological properties (Chen et al., 1992). There is also interest in the use of nitrogen plasmas to create nanoparticles of structural ceramics, such as aluminum nitride (David et al., 1990) and silicon nitride (Anderson et al., 1989; Lee et al., 1990). Nanoparticles of this material are potentially "superplastic," and hence can be used to fabricate ceramic parts via an injection molding approach. This represents great potential cost savings relative to machining.

The model presented here is only of the neutral species subsystem of the nitrogen afterglow. The behavior of charged species in the nitrogen afterglow has been studied in a previous article from which the electron temperature and concentration profiles required to determine the rate of nitrogen atom generation in the afterglow were taken (Wei et al., 1995). It was found that a model employing parameters available in the literature predicted nitrogen-atom (N-atom) flux profiles that closely agreed with those determined experimentally. Other issues studied included the modification of plasma parameters by N-atom flux measurements, the relative importance of wall and homogeneous reactions, as well as the relative importance of convective and diffusive transport.

Experimental Method and Results

Plasma reactor

The microwave system used in the present system is a 250-W commercial system (AsTex, MA.) with a three-stub tuner and a coupler with a 2.5-cm-dia. slot for a quartz flow tube. Nitrogen (Matheson, 99.999%) flow rates were controlled with calibrated rotameters. Pressure was measured with a baratron pressure gauge upstream from the plasma, and flow rate and pressure were controlled with a one-inch steel throat valve just upstream from a one-stage, Fomblin oil 75 L/min rotary vane pump (Alcatel).

The distance between the single probe input port (titrating gas, Langmuir Probe or thermocouple) and microwave coupler was varied by adjusting the coupler height with a lab jack. A more detailed description of the experimental system is available elsewhere (Chou and Phillips, 1990).

Gas temperature measurement

The temperature profile of the neutral system was measured with both a glass-covered Chromel–Alumel thermocouple, and a thermocouple placed directly in the plasma. The first method probably yields temperature readings that are slightly low, but the second method is uncertain because of the undetermined influence of charged species on the voltage reading. Thus, the absolute temperature values used are considered to be at best approximate, but the measured trend in temperature is considered reliable. Both temperature profiles were fitted with an exponential as a function of distance from microwave coupler, and these functions were used in all computations (Figure 1).

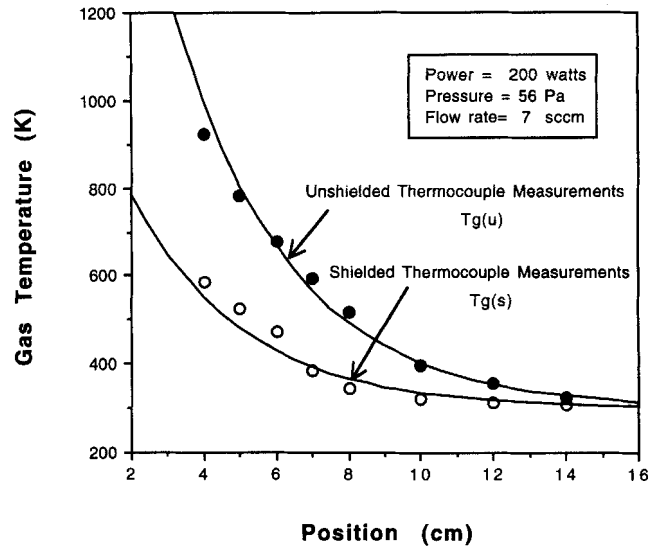

Figure 1. Gas temperature.

Gas temperature was measured both with a glass-covered thermocouple inserted into the plasma (○) and with an exposed thermocouple (●). The parameters of the fitting curves are given in Table 1.

Electron properties measurements

The temperature and density of charged species were measured with a Longmuir double probe, as described elsewhere (Wei et al., 1995). Electron temperature was calculated using Swift and Schwar's formula (1969) and fitted as a function of distance (Figure 2). Charged-species concentrations (Figure 3) were computed using Chen's empirical model (1965).

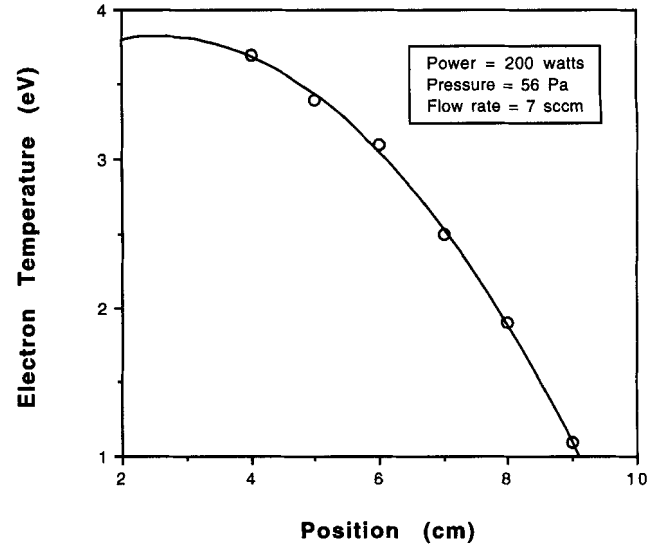

Figure 2. Electron temperature.

Electron temperature was measured using a Langmuir probe according to the standard method (Swift and Schwar, 1969). The parameters of the fitting curve are given in Table 1.

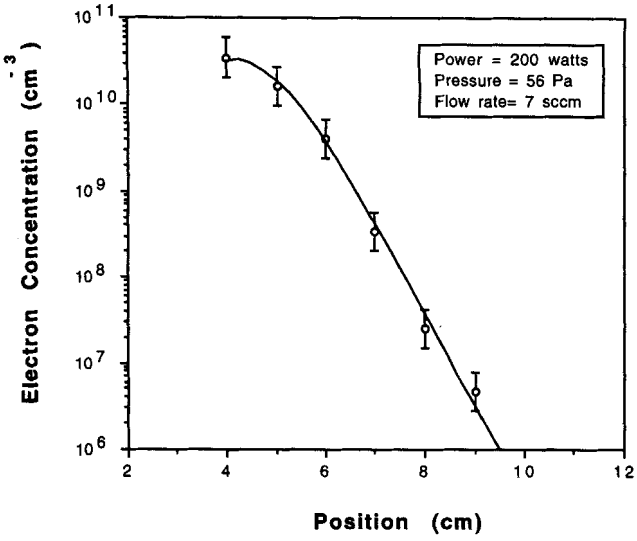

Figure 3. Electron concentration.

Electron concentration is computed from Langmuir probe data using Chen's formula (1965). Error bars represent the uncertainty in the identity of the nitrogen ions in the system. The upper and lower bounds were determined from the limiting assumptions of pure N_4^+ and N^+. Note that the charged particle concentration is orders of magnitude smaller than the N-atom concentration (see Figure 10). The parameters of the fitting curves are given in Table 1.

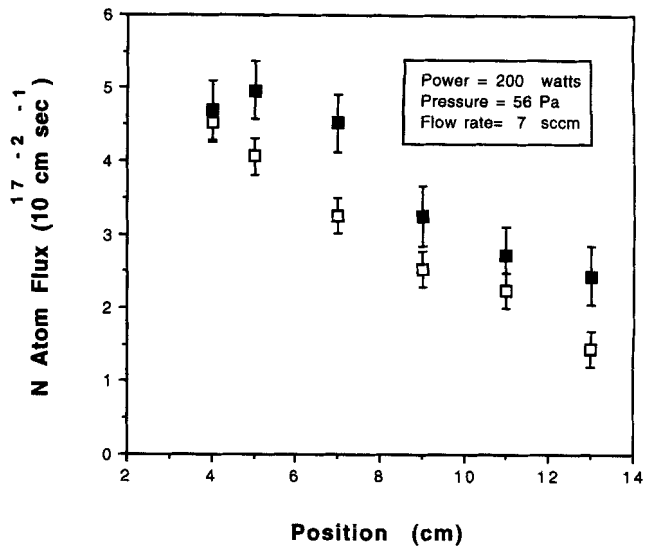

Figure 4. Nitrogen-atom flux profile.

N-atom flux was measured using chemical titration. Shown are the maximum (■) and minimum (□) measurements obtained by multiple observers. The error bars indicate that the precision for any single observer is about 10%.

The identity of the ions is a necessary input for the interpretation of the Langmuir data. Unfortunately a nitrogen plasma has four positively charged ions, N^+, N_2^+, N_3^+, and N_4^+, which cannot be distinguished by the present experimental technique. As can be seen in Figure 3, the open circles represent the electron density data if N_2^+ ions are the dominating charged species. Two extreme cases: (1) all N^+, and (2) all N_4^+ ions, were considered as the bounds of accuracy as they bracket the most physically realistic case. The modeling curve is used in later calculations.

N-atom flux

N-atom flux was measured using NO titration (Mannella, 1963; Wright and Winkler, 1968; Meikle and Hatanaka, 1989). The following reactions take place when NO is added to the afterglow:

$$NO + N \rightarrow N_2 + O \quad (1)$$

$$O + N \rightarrow NO + h\nu \quad (2)$$

The first reaction is much faster than the second, thus if the NO flux is equal to or greater than the N flux, the second reaction, which yields a lavender glow, does not take place. However, if the NO flux exceeds that of N-atom flux, a third and very slow reaction takes place:

$$NO + O \rightarrow NO_2 + h\nu. \quad (3)$$

This reaction yields a green glow. Thus, N-atom flux is determined by gradually increasing the NO flux until the afterglow changes from a lavender to clear and then to a greenish color. The NO flux and N-atom flux are approximately equal when the plasma is clear rather than lavender or green. In practice it is somewhat difficult to make this determination precisely, and thus multiple observers were used. A band representing maximum and minimum observed values is given in Figure 4. Fortunately, the spread in observed values was not large, and the trends in values were consistent. It was also found that any single observer consistently reported the same flux values ($\pm 10\%$). Prior studies using a photoelectrical monitor to detect the titration end point reported a similar level of error (Yang and Niemczyk, 1986).

Studies of N-atom flux were conducted not only as a function of position, but also as a function of microwave power, pressure, and flow rate. For these observations a single observer was used to ensure consistent relative values.

At fixed values of flow rate and pressure, N-atom flux was found to increase with increasing absorbed microwave power (Figure 5a). In contrast, the N-atom yield (defined as grams per kilowatt hour) decreased (Figure 5b). No data for direct comparison with other nitrogen afterglows are available, but reports on oxygen plasmas vary. The results reported here are consistent with those of Bell and Kwong (1972) at low power (80–140 W), but Brake et al. (1983) found that O-atom yield increased with power (400–700 W), and Mearns and Morris (1971) measured constant yield (100–400 W).

As generally reported (Mearns and Morris, 1971; Bell and Kwong, 1972; Brake et al., 1983; Sabadil and Pfau, 1985; Meikle and Hatanaka, 1989), N-atom flux increases as pressure is reduced at constant power and flow rate (Figure 5a and 5b). As pressure decreases, both electron temperature and concentration increase, which results in a higher rate of N-atom generation via electron dissociation.

The N-atom flux was found to increase with increasing flow rates for fixed power and pressure (Figure 6). Once again, no results are available for direct comparison with other nitrogen afterglows. Also, there is no agreement on the impact of flow rate on the yield of oxygen atoms in an oxygen after-

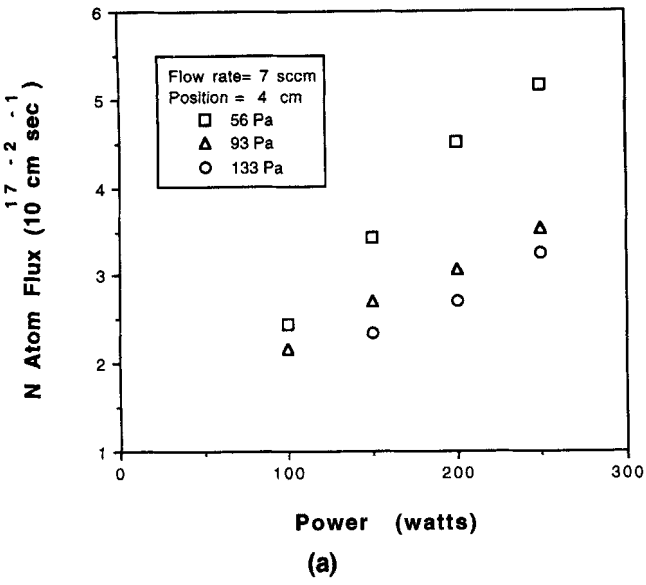

Figure 5. Power and pressure dependencies.

Shown are the power and pressure dependence on (a) N-atom flux and (b) N-atom yield. An increase in microwave power results in an increase in N-atom flux measurements but a lower N-atom yield. At higher pressures both N-atom flux and yield are smaller.

glow. Brake et al. (1983) found that an increased flow rate led to an increased O-atom yield, whereas Bell and Kwong (1972) found that flow rate had no impact on O-atom yield.

Model

A mathematical model of the N-atom flux and concentration profiles in the afterglow region of the microwave plasma is developed below and the predicted profiles compared with the measured profiles described earlier. The axisymmetric model accounts for axial temperature gradients, homogeneous and heterogeneous kinetics, convection, and mass diffusion in both the radial and axial directions.

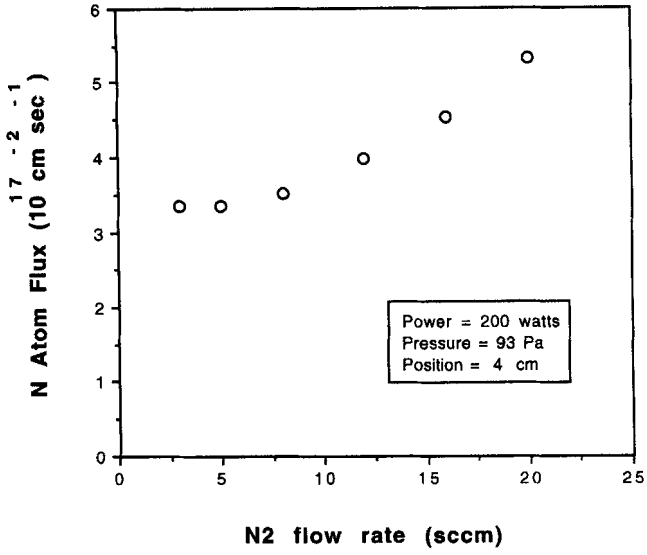

Figure 6. Flow rate dependence.

N-atom flux increases with increasing flow rate for fixed power and pressure.

Transport equation

Mass conservation of N atoms in an axisymmetric system can be expressed as follows:

$$\rho V\frac{\partial w_N}{\partial z}=\frac{1}{r}\frac{\partial}{\partial r}\left(r\rho\vartheta\frac{\partial w_N}{\partial r}\right)+\frac{\partial}{\partial z}\left(\rho\vartheta\frac{\partial w_N}{\partial z}\right)+R_G-R_R, \tag{4}$$

where ρ is the total mass density, V is the fluid velocity, w_N is the mass fraction of atomic nitrogen, ϑ is the mass diffusivity of N atoms, R_G is the rate of generation of N atoms, and R_R is rate of loss of N atoms due to homogeneous recombination reactions (see the following subsection, Reaction mechanism). Equation 4 assumes plug flow for the fluid velocity. Transport coefficients and reaction rates are strong functions of the species and electron temperatures. As with the earlier study for O atoms, no attempt was made to solve the simultaneous energy balance, but instead experimental profiles of the species and electron temperatures were incorporated into the model. The fluid density was determined from the gaseous temperature using the Ideal Gas Law, and the velocity from an overall mass balance, which for the present system reduces to $V=M/\rho A$, where M is the fixed mass rate of flow through the system and A is the cross-sectional area of the reactor. In addition, pressure losses in the pipe were neglected, and the bimolecular mass diffusivity of N atoms through N_2 was determined from the following expression (Hirshfelder et al., 1954):

$$\vartheta=\frac{100\sqrt{5.3/M_N}}{(\sigma_{N-N_2})^2}\frac{T^{1.5}}{P}$$

ϑ in $cm^2\cdot s^{-1}$, P in Pa, and T in K. The radial temperature gradient was assumed to be small, therefore the radial dependence of the density and diffusivity are also neglected.

Table 1. Model Parameters

Parameter	Value	Source
Pressure (P)	56 Pa (0.42 torr)	Measurement
Flow rate	7 std. cm^3	Measurement
Gas temp. (T_g)	$298+947.3\,e^{-0.33z}$ K, z in cm $298+2{,}505.7\,e^{-0.32z}$ K, z in cm	Fit of Figure 1, $T_g(s)$ curve Fit of Figure 1, $T_g(u)$ curve
Electron temp. (T_e)	$3.38+0.34z-0.066z^2$ eV, $4<z<9$ cm	Fit of Figure 2
Electron no. density (n_e)	$10^{5.38+2.96z-0.5z^2+0.02z^3}$ cm^{-3}	Fit of model results, Wei et al., 1995
Rate const. of homogeneous recomb. (k_h)	6.5×10^{-33} $cm^6\cdot s^{-1}$	Ricard et al., 1991
Wall recomb. coeff. (γ)	0.0008	Marshall, 1962
Rate const. of electron impact dissoc. (k_e)	$5.79\times10^{-9}\,e^{-11/T_e}$ $cm^3\cdot s^{-1}$	Bacri and Medani, 1980
Diffusivity (ϑ)	$5.81\,T_g^{1.5}P^{-1}$ $cm^2\cdot s^{-1}$	Hirshfelder et al., 1954

Reaction mechanism

Recombination. In the afterglow region of the plasma, both homogeneous recombination and wall recombination of N atoms take place. Homogeneous recombination is a third-order reaction expressed as

$$N+N+M\rightarrow N_2+M,$$

where M stands for a third body (any molecular species). The rate expression is given by

$$R_R=\frac{k_h\,\rho^3}{196}w_N^2. \tag{5}$$

The rate constant in the preceding reaction has been well studied (see Table 2) and there is good agreement on the value of k_h. It is also generally agreed that the homogeneous reaction of atoms is a low activation energy process. Rate constants used in the present study are summarized in Table 1.

Recombination of N atoms is also catalyzed by the tube wall. This mechanism, referred to as wall recombination, is not shown explicitly in Eq. 1, but is part of the boundary conditions (see discussion in the next subsection). Recombination of N atoms at the tube wall is assumed to be a first-order reaction

$$N+S-N\rightarrow N_2+S$$

with the following rate expression

$$R_w=\frac{k_w w_N(R)R}{2}, \tag{6}$$

where $w_N(R)$ refers to the concentration of N atoms at the wall, and k_w is the rate constant of wall recombination that can be expressed as $(\gamma\nu/2R)$ (Shuler and Laidler, 1949), where γ is the wall recombination coefficient, ν is the mean thermal velocity of the atoms, and R is the radius of the tube. The wall recombination coefficient γ on clean quartz tube has been studied by Marshall (1962). He reported values of 0.0008, 0.0007, 0.0009 at 300, 600 and 800 K, respectively. The average of Marshall's values was used in the model (see Table 1).

N-Atom Generation. Nitrogen atoms can be generated by electron impact dissociation

$$N_2+e\rightarrow N+N+e$$

and the rate can be expressed as

$$R_G=k_e n_e\,\rho(1-w_N), \tag{7}$$

Table 2. Summary of Nitrogen-Atom Recombination Studies

Material	γ (10^{-5})	$2k_2$*	$2k_n$†	Method	Reference
Quartz	80			ESR	Marshall, 1962
Quartz	60			Calorimetry	Kim and Boudart, 1991
Quartz	55, 0.7†	2.7	0.6	ESR	Evenson and Burch, 1966
Quartz	2.5‡, 0.02†,‡	0.35	2.25	ESR	Evenson and Burch, 1966
Pyrex	7.5		2.9	Titration	Mavroyannis and Winkler, 1961
Pyrex	0.32		0.72	Mass Spectrometry	Yamashita, 1979
Pyrex			0.65	Titration, OES	Ricard et al., 1991
Pyrex		3.3	0.76	OES	Clyne and Stedman, 1967
Pyrex		1.44	0.77	Titration, OES	Campbell and Thrush, 1967
Mo glass		15,000		Time Delay	Markovic et al., 1994

*In unit 10^{-15} $cm^3\cdot s^{-1}$
**In unit 10^{-32} $cm^6\cdot s^{-1}$
†Nitrogen gas containing 0.7% oxygen.
‡Static nitrogen afterglow.

where n_e is the electron concentration and k_e is the rate constant of electron impact dissociation. The electron concentration (n_e) is fitted from a numerical solution of a previous study (Wei et al., 1995), while k_e can be calculated from the integration of the electron energy distribution and the dissociation cross section. The computation by Bacri and Medani (1980) indicates that the rate constant is a strong function of electron temperature. Taking the values they reported and fitting with Arrhenius' Law, it is shown in the present work that the activation energy of the preceding reaction is 11 eV. Expressions for n_e and k_e are shown in Table 1.

Boundary conditions

The boundary conditions for Eq. 4 in the z-direction have been determined experimentally. At the entrance to the afterglow region, the flux is fixed to equal the measured value (see the earlier subsection titled Transport equation), and far downstream the effect of the plasma is lost and the N-atom concentration approaches zero. In the radial direction, the gradient is zero along the centerline because of symmetry, and the flux at the wall is balanced by the wall recombination rate. Mathematically this becomes

$$\begin{aligned} z=4 \quad & \rho V w_N - \rho\vartheta\frac{\partial w_N}{\partial z} = J_0 \\ z=\infty \quad & w_N = 0 \\ r=0 \quad & \frac{\partial w_N}{\partial r} = 0 \\ r=R \quad & -\vartheta\frac{\partial w_N}{\partial r} = \frac{k_w w_N R}{2}, \end{aligned} \tag{8}$$

where J_0 is the measured flux at the entrance.

Axial profile

Equations 4–7 and the boundary conditions (Eq. 8) constitute the model for the N-atom concentration in the afterglow region of the plasma; however, the axial dependence of the N-atom concentration can be determined with a simpler model by solving for the *mixed mean* radial value of w_N. It is convenient to define a pth-order radial moment of the mass fraction of N atoms by the following integral:

$$\overline{w_N^p} = \frac{2}{R^2}\int_0^R w_N^p(r,z)r \quad dr,$$

where p is a fixed power. A transport equation for the mixed mean mass fraction ($\overline{w_N}$) can be found by integrating Eq. 4 over the radius of the tube. The resulting *exact* expression is

$$\rho V\frac{d\overline{w_N}}{dz} = \frac{d}{dz}\left(\rho\vartheta\frac{d\overline{w_N}}{dz}\right) + k_e n_e \rho(1-\overline{w_N}) - \frac{k_h \rho^3}{196}\overline{w_N^2} - k_w \rho w_N(R). \tag{9}$$

Note that an explicit wall recombination term is present in Eq. 9 (last term on the righthand side) resulting from the integral of the radial diffusion term evaluated at the wall. In principle Eq. 9 can be integrated to obtain the axial dependence of the mean mass fraction; however, the final two terms on the righthand side are functions of the radial distribution of N atoms, which at present is unknown. An approximate radial analysis is now introduced to estimate the significance of the radial distribution on the overall transport of N atoms.

Assumptions and simplifications

The exact radial behavior of w_N can be determined from the two-dimensional solution of Eq. 4; however, the magnitude of the radial gradient can be estimated from an approximate analysis used frequently in heat transfer (Siegel et al., 1958). The assumption is based on the concept that for fully developed flows and nearly fully developed mass transfer, axial gradients are not strong functions of the radial coordinate. This approximation is accurate at asymptotically large distances downstream from the coupling region; however, in many flows it can be shown to be a good approximation even at short distances. Mathematically the approximation can be written as

$$\frac{\partial w_N}{\partial z} \approx \frac{d\overline{w_N}}{dz}.$$

Introducing this assumption into the original governing equation (Eq. 4) and simplifying using the mixed mean transport equation (Eq. 9) yields the following approximate expression for the radial distribution

$$\frac{1}{r}\frac{\partial}{\partial r}\left(r\rho\vartheta\frac{\partial w_N}{\partial r}\right) + k_e n_e \rho(\overline{w_N} - w_N) + k_w \rho w_N(R) + \frac{k_h \rho^3}{196}\left(\overline{w_N^2} - w_N^2\right) = 0. \tag{10}$$

Equation 10 is an *ordinary* differential equation for the radial profile of w_N at a given axial location, subject to the same boundary conditions as shown in Eq. 8. Numerical analysis of Eq. 10 demonstrated that homogeneous recombination was negligible as compared to wall recombination, suggesting we neglect the final term on the lefthand side. It should be noted that although homogeneous recombination is negligible in the present application, it can become appreciable at higher pressures (> 2 torr). With this additional approximation, Eq. 10 is reduced to the following linear equation:

$$\frac{1}{r}\frac{\partial}{\partial r}\left(r\rho\vartheta\frac{\partial w_N}{\partial r}\right) + k_e n_e \rho(\overline{w_N} - w_N) + k_w \rho w_N(R) = 0, \tag{11}$$

which has the following general solution

$$w_N\left(\frac{r}{R}, z\right) = \overline{w_N}(z) + \frac{\beta}{\alpha}w_N(1,z) + CI_0\left(\alpha^{1/2}\frac{r}{R}\right), \tag{12}$$

where $I_0(y)$ is the modified Bessel function, and the dimensionless parameters α and β are defined as

$$\alpha = \frac{k_e n_e R^2}{\vartheta} \quad \text{and} \quad \beta = \frac{k_w R^2}{\vartheta}.$$

The constants C and $w_N(1,z)$ can be evaluated from a consistency condition at $r/R = 1$ and the boundary condition at the wall. The quantity of interest is the mass fraction at the wall $w_N(1,z)$ as a function of the mixed mean mass fraction $\overline{w}_N(z)$ (see Eq. 9). For the range of values of α and β of interest, that relationship reduces to the following expression

$$w_N(1,z) = \frac{\overline{w_N}(z)}{1+(\beta/8)}. \tag{13}$$

The Damköhler Group, β, is a measure of relative importance of wall recombination to diffusion. Although wall recombination is significant, the diffusivity of N atoms at low pressure is so large that values of β in the present system are found to vary between 0.03 and 0.08, corresponding to differences between the mixed mean value and the wall value that never exceed 1%. Clearly the effect of the radial gradients in Eq. 9 can be neglected. This confirms the assumption used in several previous studies and justifies the reduction of Eq. 4 to an ordinary differential equation (Eq. 9). It should be noted that Kaufman (1961) arrived at a similar relationship to Eq. 13 based on arguments that were less general than those presented here.

Numerical method

Based on the results in the previous section, Eq. 9 was reduced to the following simplified form

$$\rho V \frac{d\overline{w_N}}{dz} = \frac{d}{dz}\left(\rho\vartheta \frac{\partial \overline{w_N}}{\partial z}\right) + k_e n_e \rho(1-\overline{w_N}) - \frac{k_h \rho^3}{196}(\overline{w_N})^2 - k_w \rho \overline{w_N}, \tag{14}$$

where radial gradients of w_N have been neglected. A finite-difference method was used to solve Eq. 14. The boundary condition listed at $z = \infty$ was replaced by a more practical boundary condition set at a value of z that was at least $10L$ downstream from the entrance, where L is the characteristic axial length for decay defined as $L = (k_w/V)$. Numerical experimentation with longer distances produced negligible differences in the results. All the model parameters are listed in Table 1.

Model Results

It can clearly be seen in Figure 7 that there is good agreement between the model and the experimental data. Two modeling curves are shown, which represent the two different gas temperatures that were used. As described in the experimental section, there are uncertainties in the measurement of gas temperature (Figure 1). Clearly, both curves are relatively close, indicating that the uncertainties encountered in determining gas temperature have little impact on the model.

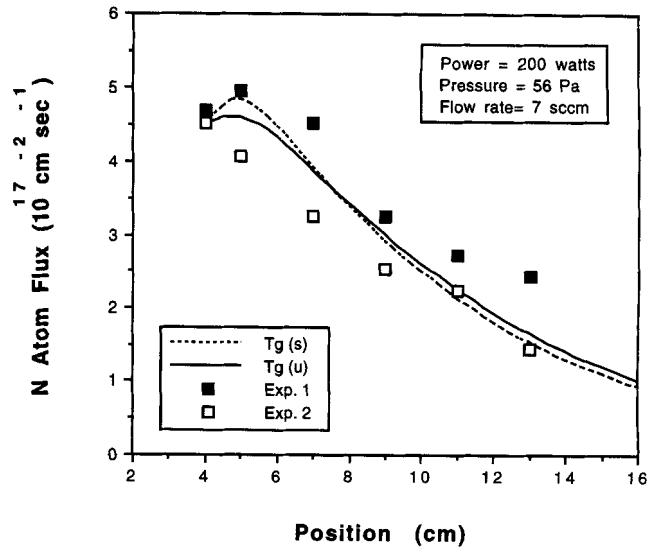

Figure 7. Model results.

Shown are the comparisons of modeling results and experimental measurements. Two modeling curves, which represent the two different gas temperatures (Figure 1) that were used, are shown.

One benefit of an accurate model is that it allows one to study the impact of independent variation of parameters that are difficult to uncouple experimentally. In this study an effort was made to independently assess the impact of a number of effects, including the diffusive and convective flux, heterogeneous and homogeneous reactions, radical generation in the afterglow, and the impact of the titration of radicals on the actual flux profile.

Dominant kinetics

Qualitatively it is clear that generation of N atoms in the afterglow only marginally impacts the flux. As can be seen in Figure 8, if the generation term is neglected, the predicted value of N-atom flux still falls in the range of experimental values.

Wall recombination is the most important N-atom recombination process. Figure 8 also shows that neglecting wall recombination yields N-atom flux values far higher than those measured experimentally. In contrast, homogeneous recombination is insignificant and can be neglected. In fact, there is no visual difference in the modeling results if all the homogeneous recombination terms are ignored. This certainly suggests that if high N-atom concentrations are required for a particular process, then efforts must be made to reduce the rate of wall recombination. Indeed, metaphosphoric acid is often coated on the tube wall to prevent appreciable N-atom surface recombination (Young, 1961; Clyne and Stedman, 1967).

Since the model result is most sensitive to the wall recombination rate, the selection of the wall recombination coefficient (γ) can be critical. As summarized in Table 2, prior studies showed that γ for N atoms is a strong function of the material of the wall, the oxygen impurity, the flow type, and

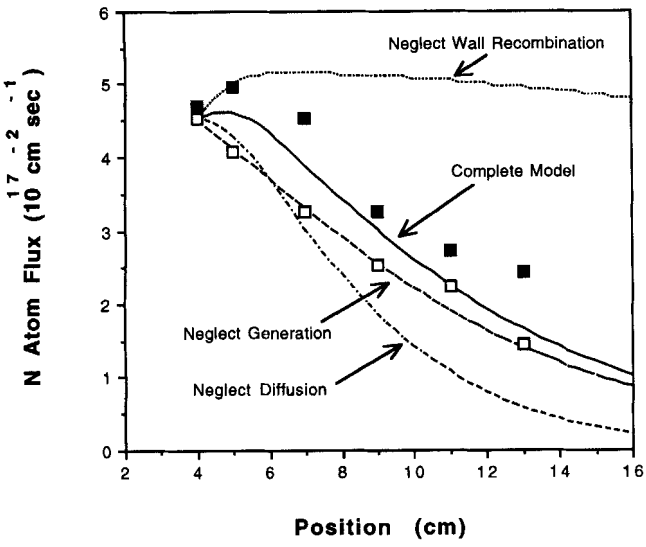

Figure 8. Sensitivity test.

Relative importance of wall recombination, homogeneous recombination, N-atom generation, and diffusion on model results are shown and compared with experimental data.

surface roughness (Kim and Boudart, 1991). For N-atom recombination, the reported values of γ on quartz are an order of magnitude higher than that on Pyrex, and γ in flowing nitrogen is an order of magnitude higher than that in nonflowing nitrogen (Evenson and Burch, 1966). As illustrated in Figure 9, using the rate constants measured on Pyrex (Mavroyannis and Winkler, 1961) resulted in model values of N-atom flux much higher than the measured values. In contrast, the rate constants reported for quartz yield excellent agreement with the experiment (Marshall, 1962; Evenson and Burch, 1966). Thus, the present results are found to be in good quantitative agreement with earlier studies regarding the value of the wall recombination coefficient for quartz.

A second issue regarding the recombination process at the quartz surface is the mechanism. Indeed, the reaction mechanism for N-atom recombination at the reactor wall has been a matter of dispute for many years. In this article, as in many previous studies, the process is assumed for simplicity to be first order, and excellent agreement with experiment is obtained. However, many workers argued that the process is second order (Campbell and Thrush, 1967; Clyne and Stedman, 1967; Markovic et al., 1994). Figure 9 shows that both first- and second-order models are able to accurately explain the data obtained. Yet it should be noted that no second-order rate constant (k_2) for N-atom recombination on quartz is available in the literature. The value for k_2 ($2.4 \pm 0.5 \times 10^{-14}$ $cm^3 \cdot s^{-1}$) employed in the present work was obtained from a best fit to the experiment data. The values for k_2 previously available are for Pyrex (Clyne and Stedman, 1967) and are inadequate (Figure 9). This is consistent with the general understanding that second-order wall recombination is material sensitive (Markovic et al., 1994). In sum, the present study provides no basis for resolving the issue of the order of the N-atom recombination process at the surface.

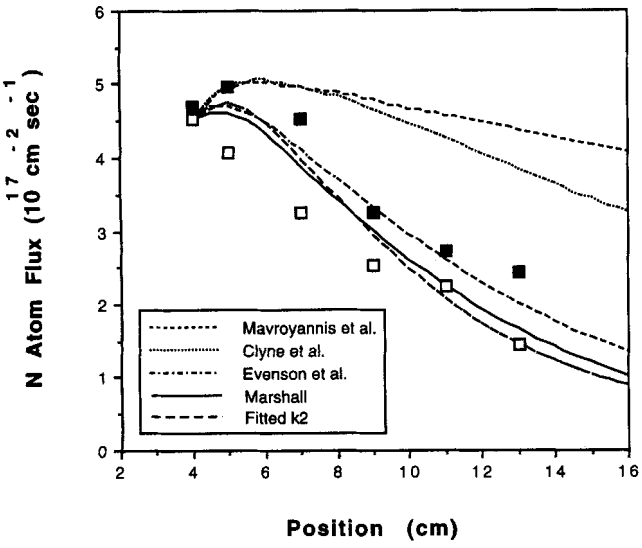

Figure 9. Wall recombination.

The rate of wall recombination has a profound influence on the model results. Using the rate constants reported by Marshall (1962) and Evenson and Burch (1966) for quartz surfaces yielded good agreement with experimental measurements. Model results using the rate constants for Pyrex (Mavroyannis and Winkler, 1961; Clyne and Stedman, 1967) yielded poor agreement. A second-order model, with a best-fit rate constant (fitted k_2), worked as well.

Diffusion

It is clear that diffusion plays an important role in transport. As shown in Figure 8, if diffusion is neglected, the flux values are always lower than the measured values. However, it is shown in Figure 10 that the mass fraction and concentration of N atoms are higher if diffusion is neglected. Moreover, it can be seen that diffusion "smooths out" the concentration profile peak.

One possibly unexpected finding is that there is a peak in concentration about 8.5 cm below the coupler (Figure 10). A similar concentration profile found in the O-atom model

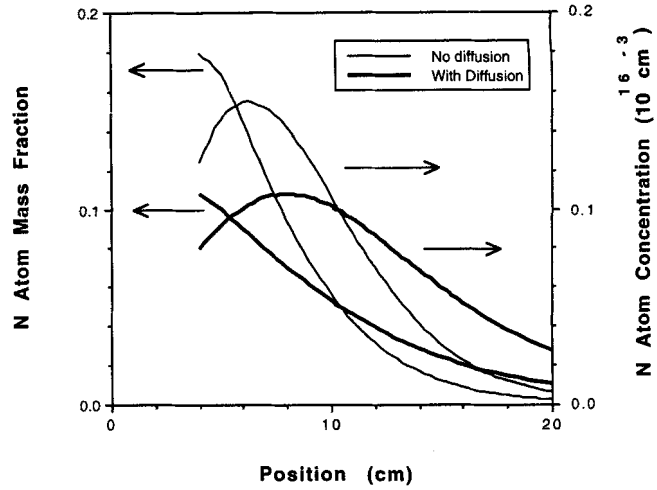

Figure 10. Axial diffusion.

The mass fraction and concentration of N atoms are higher if diffusion is neglected (thinner curves). It can also be seen that diffusion "smooths out" the concentration profile peak.

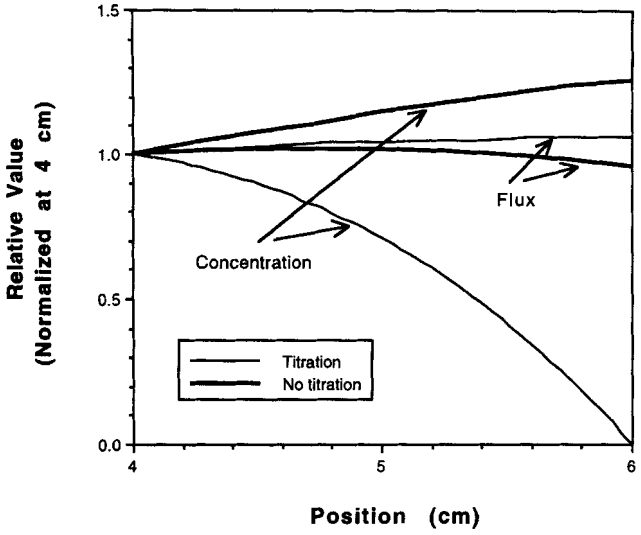

Figure 11. Titration.

Titrating the plasma with NO modifies the transport processes, dramatically changing the concentration profile, but only slightly impacting the flux. The thinner curves are for the case in which titration results in zero concentration 6 cm below the coupler.

(Chou et al., 1992) shows that the peak in concentration results from the steep temperature profile in the region below the coupler. As the gas cools, it occupies a smaller volume, resulting in increased concentration. The temperature profile is responsible for the position and size of the peak in the N-atom concentration profile as well. A constant temperature profile was input to the model (not shown) and yielded a concentration peaked at 5 cm below the coupler, similar in shape and at the same point at which there is a peak in flux due to N-atom generation (Figure 9).

Titration

In addition to the uncertainty in the N-atom profile that results from a difficulty in determining the precise point at which the afterglow is "clear" (see experimental section), there is an uncertainty introduced by titration itself. Titration changes the boundary conditions, which naturally impacts diffusion. Indeed, titrating to the "end point" of N-atom concentration sharply increases the N-atom concentration gradient just above the titration point. This will result in an increased rate of diffusive mass transport.

The model was used to assess the impact of the measurement technique on the values measured. A new zero point, just 6 cm below the coupler was employed. A point close to the coupler was selected, as the largest error due to titration should occur in a position at which the concentration gradient will most sharply increase. The impact of temperature differences between titrating gas and afterglow, back diffusion of the titrating gas, and so forth, are not included in the model. Thus, this only models an idealized experiment in which NO is used to titrate N to its zero point at this same location.

The results of this effort (Figure 11) show that the flux profile is not strongly impacted, although the concentration profile is significantly modified in the present work. The reason flux is not strongly impacted is that one resulting process tends to increase flux, and a second tends to decrease flux. That is, the diffusive flux is increased because the concentration profile is steeper. However, the convective flux is lowered because the overall concentration in the region above the titrating point is reduced. The two processes are almost of equal magnitude in the present system, such that the net impact of titration on flux is minimal. This result suggests that the error intrinsic to the titration method is less than the experimental error.

Summary

The afterglow region of a steady-state, low-pressure, nonisothermal microwave-generated nitrogen plasma was characterized. Nitrogen atom flux was measured as a function of distance from the coupler. The influence of power, pressure, and flow rate on the plasma were studied. It was found that an increase in power or flow rate, or a decrease in pressure resulted in increased production of N atoms.

A continuum model was developed to predict N atoms behavior in an afterglow plasma. A pseudo fully developed approximation was used to show that radial dependence of N atoms was insignificant, which reduced the model to a one-dimensional mass continuity equation. Measured temperature profiles and electron concentration profiles were input to the model. It was shown that the model, with no adjustable parameters, and all rate constants from the literature, yields very good agreements with experimental measurements. It was also shown that diffusion and wall recombination play important roles in the model, N-atom generation marginally impacts the flux, but homogeneous recombination is so insignificant that it can be neglected. The model was manipulated to assess the impact of chemical titration. It was found that the N-atom flux profile was only slightly impacted under operating conditions typically employed, although the concentration profile was strongly modified.

Notation

e = electron
r = radial coordinate, cm
R_w = rate of wall recombination of N atoms, $g \cdot cm^{-3} \cdot s^{-1}$
z = axial coordinate, cm

Literature Cited

Anderson, A., T. T. Kodas, and D. M. Smith, "Vapor-Phase Processing of Powders: Plasma Synthesis and Aerosol Decomposition," *Ceram. Bull.*, **68**, 996 (1989).

Bacri, J., and A. Medani, "Electron Diatomic Molecule Weighted Total Cross Section Calculation. II. Application to the Nitrogen Molecule," *Physica C*, **101**, 410 (1980).

Bell, A. T., and K. Kwong, "Dissociation of Oxygen in a Radiofrequency Electrical Discharge," *AIChE J.*, **18**, 990 (1972).

Bougdira, J., G. Henrion, M. Fabry, M. Remy, and J. R. Cussenot, "Low Frequency d.c. Pulsed Plasma for Iron Nitriding," *Mat. Sci. Eng.*, **A 139**, 15 (1991).

Brake, M. L., J. Hinkle, J. Asmussen, M. Hawley, and R. L. Kerber, "Dissociation and Recombination of Oxygen Atoms Produced in a Microwave Discharge: I. Experiment," *Plasma Chem. Plasma Proc.*, **3**, 63 (1983).

Campbell, I. M., and B. A. Thrush, "The Recombination of Nitrogen Atoms and the Nitrogen Afterglow," *Proc. R. Soc. London. A*, **296**, 201 (1967).

Chen, F. F., "Saturation Ion Currents to Langmuir Probes," *J. Appl. Phys.*, **36**, 675 (1965).
Chen, M. Y., X. Lin, V. P. Dravid, Y. W. Chung, M. S. Wong, and W. D. Sproul, "Growth and Characterization of C-N Thin Films," *Surf. Coating Technol.*, **54/55**, 360 (1992).
Chou, C. H., and J. Phillips, "Platinum Metal Etching in a Microwave Oxygen Plasma," *J. Appl. Phys.*, **68**, 2415 (1990).
Chou, C. H., T. C. Wei, and J. Phillips, "Detailed Model of the Afterglow Region of a Microwave Generated Oxygen Plasma," *J. Appl. Phys.*, **72**, 870 (1992).
Clyne, M. A. A., and D. H. Stedman, "Rate of Recombination of Nitrogen Atoms," *J. Phys. Chem.*, **71**, 3071 (1967).
Dautremont-Smith, W. C., "Damage and Surface Modification Produced by Plasma Processing," *Proc. 6th Symp. Plasma Processing*, G. S. Mathod, G. C. Schwartz, and R. A. Gottscho, eds., The Electrochemical Society, San Diego, p. 338 (1987).
David, M., S. V. Babu, and D. H. Rasmussen, "RF Plasma Synthesis of Amorphous AlN Powder and Films," *AIChE J.*, **36**, 871 (1990).
Evenson, K. M., and D. S. Burch, "Atomic Nitrogen Recombination," *J. Chem. Phys.*, **45**, 2450 (1966).
Graves, D. B., "Plasma Processing in Microelectronics Manufacturing," *AIChE J.*, **35**, 1 (1989).
Han, H. X., and J. Feldman, "Structural and Optical Properties of Amorphous Carbon Nitride," *Solid State Commun.*, **65**, 921 (1988).
Harteck, P., R. R. Reeves, and G. Mannella, "Rate of Recombination of Nitrogen Atoms," *J. Chem. Phys.*, **29**, 608 (1958).
Herron, J. T., J. L. Franklin, P. Bradt, and V. H. Dibeler, "Kinetics of Nitrogen Atom Recombination," *J. Chem. Phys.*, **30**, 879 (1959).
Hirshfelder, J., C. Curtis, and B. Bird, *Molecular Theory of Gases and Liquids*, Wiley, New York (1954).
Hochgreb, S., and F. L. Dryer, "A Comprehensive Study on CH_2O Oxidation Kinetics," *Combust. Flame*, **91**, 257 (1992).
Kaufman, F., "Reactions of Oxygen Atoms," *Progress in Reaction Kinetics*, G. Porter and B. Stevens, eds., Pergamon, New York, p. 1 (1961).
Kim, Y. C., and M. Boudart, "Recombination of O, N, and H Atoms on Silica: Kinetics and Mechanism," *Langmuir*, **7**, 2999 (1991).
Kretschmer, C. B., and H. L. Petersen, "Kinetics of Three-Body Atom Recombination," *J. Chem. Phys.*, **39**, 1772 (1963).
Lee, H. J., K. Eguchi, and T. Yoshida, "Preparation of Ultrafine Silicon Nitride, and Silicon Nitride and Silicon Carbide Mixed Powders in a Hybrid Plasma," *J. Amer. Ceram. Soc.*, **73**, 3356 (1990).
Mannella, G., "Active Nitrogen," *Chem. Rev.*, **63**, 1 (1963).
Markatou, P., L. D. Pfefferle, and M. D. Smooke, "A Computer Study of Methane-Air Combustion over Heated Catalytic and Non-Catalytic Surfaces," *Combust. Flame*, **93**, 185 (1993).
Markovic, V. L., Z. L. Petrovic, and M. M. Petrovic, "Surface Recombination of Atoms in a Nitrogen Afterglow," *J. Chem. Phys.*, **100**, 8514 (1994).
Marshall, T., "Surface Recombination of Nitrogen Atoms upon Quartz," *J. Chem. Phys.*, **37**, 2501 (1962).
Mavroyannis, C., and C. A. Winkler, "The Reaction of Nitrogen Atoms with Oxygen Atoms in the Absence of Oxygen Molecules," *Can. J. Chem.*, **39**, 1601 (1961).
Mearns, A. M., and A. J. Morris, "Oxidation Reactions in a Microwave Discharge: Factors Affecting Efficiency of Oxygen Atom Production," *Chem. Eng. Prog. Symp. Ser.*, **67**, 37 (1971).
Meikle, S., and Y. Hatanaka, "Measurements of the Atomic Nitrogen Population Produced by a Microwave Electron Cyclotron Resonance Plasma," *Appl. Phys. Lett.*, **54**, 1648 (1989).
Mellouki, A., G. Le Bras, and G. Poulet, "Discharge Flow Kinetic Study of NO_3 Reactions with Free Radicals: The Reactions of NO_3 with Cl," *J. Phys. Chem.*, **91**, 5760 (1987).
Nichollian, E. H., and J. R. Brews, *MOS Physics and Technology*, Wiley, New York (1980).
Niu, C., Y. Z. Lu, and C. M. Lieber, "Experimental Realization of the Covalent Solid Carbon Nitride," *Science*, **261**, 334 (1993).
Ricard, A., J. E. Oseguera-Pena, L. Falk, H. Michel, and M. Gantois, "Active Species in Microwave Postdischarge for Steel-Surface Nitriding," *IEEE Trans. Plasma Sci.*, **PS-18**, 940 (1990).
Ricard, A., J. Tetreault, and J. Hubert, "Nitrogen Atom Recombination in High Pressure Ar-N2 Flowing Post-Discharges," *J. Phys. B: At. Mol. Opt. Phys.*, **24**, 1115 (1991).
Sabadil, H., and S. Pfau, "Measurements of the Degree of Dissociation in Oxygen DC Discharges: Comparison of the Ozone Method with the Wrede-Harteck Method," *Plasma Chem. Plasma Proc.*, **5**, 67 (1985).
Shuler, K. E., and K. L. Laidler, "The Kinetics of Heterogeneous Atom and Radical Reactions: I. The Recombination of Hydrogen Atoms on Surfaces," *J. Chem. Phys.*, **17**, 1212 (1949).
Siegel, R., E. M. Sparrow, and T. M. Hallman, "Steady Laminar Heat Transfer in a Circular Tube with Prescribed Wall Heat Flux," *Appl. Sci. Res. A.*, **7**, 3886 (1958).
Strite, S., and H. Morkoc, "GaN, AlN, and InN: A Review," *J. Vac. Sci. Technol. B*, **10**, 1237 (1992).
Sun, Y. M., and J. G. Ekerdt, "Electron-Induced Nitridation of GaAs(100) with Ammonia," *J. Vac. Sci. Technol. B*, **11**, 610 (1993).
Swift, J. D., and M. J. R. Schwar, *Electrical Probes for Plasma Diagnostics*, Elsevier, New York (1969).
Wei, T. C., L. R. Collins, and J. Phillips, "Dynamics of Charged Species in the Afterglow Region of a Low-Pressure Microwave Plasma," *J. Phys. D: Appl. Phys.*, **28**, 295 (1995).
Wright, A. W., and C. A. Winkler, *Active Nitrogen*, Academic Press, New York (1968).
Yamashita, T., "Rate of Recombination of Nitrogen Atoms," *J. Chem. Phys.*, **70**, 4248 (1979).
Yang, H. C., and T. M. Niemczyk, "Determination of Nitrogen Atom Concentration in Flowing Gases," *Anal. Chem.*, **58**, 2492 (1986).
Young, R. A., "Pressure Dependence of the Absolute Catalytic Efficiency of Surfaces for Removal of Atomic Nitrogen," *J. Chem. Phys.*, **34**, 1292 (1961).

Manuscript received Mar. 29, 1995, and revision received July 31, 1995.